Supplement of Geosci. Model Dev., 16, 1–15, 2023
https://doi.org/10.5194/gmd-16-1-2023-supplement

Geoscientific Model Development
Open Access
EGU

Supplement of

Towards an improved representation of carbonaceous aerosols over the Indian monsoon region in a regional climate model: RegCM

Sudipta Ghosh et al.

Correspondence to: Sagnik Dey (sagnik@cas.iitd.ac.in)

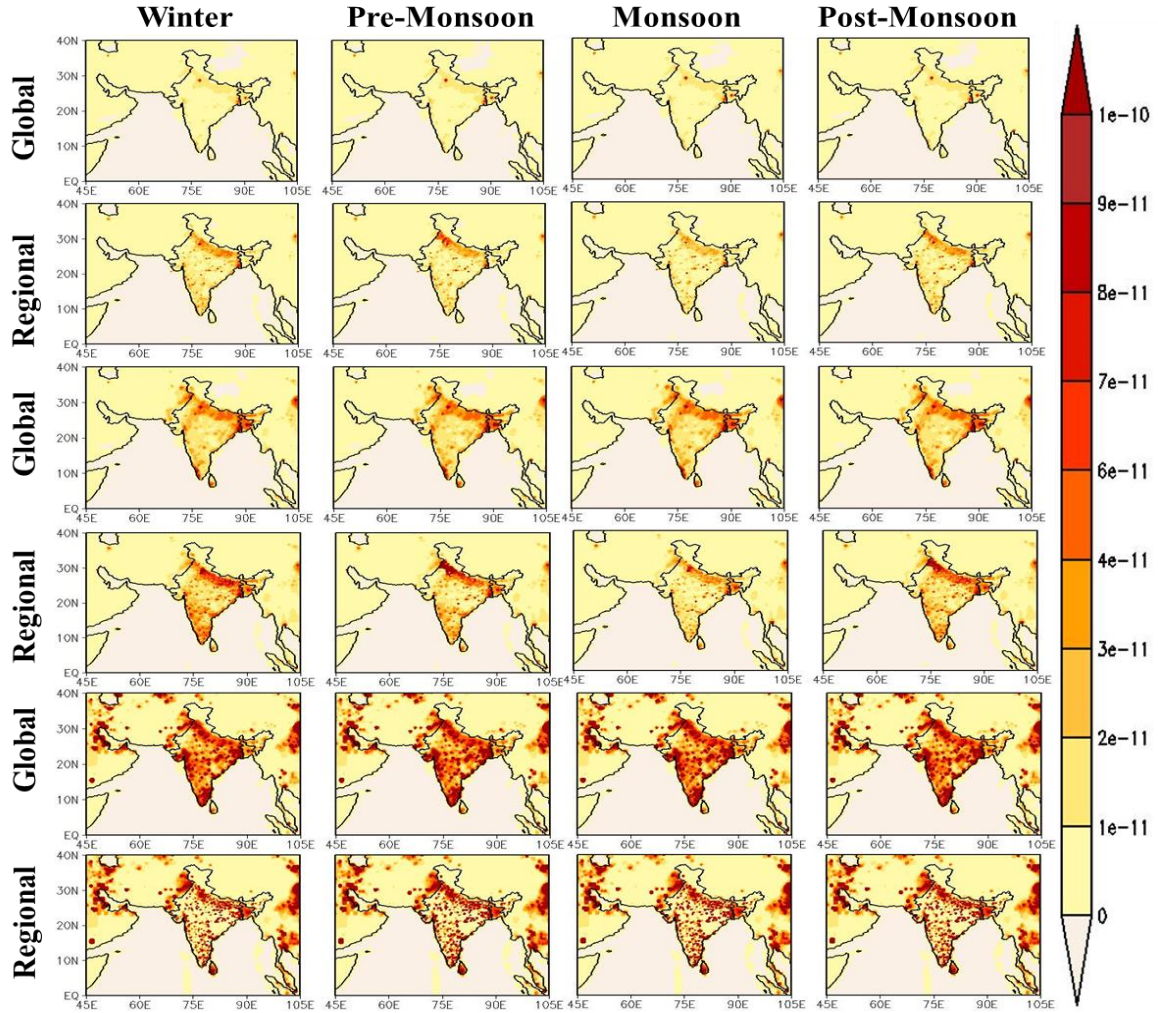

Figure S1. Seasonal variation of the global and regional emission inventories in kg m^{-2} s^{-1} for BC (1st and 2nd rows), OC (3rd and 4th rows) and SO_2 (5th and 6th rows) used in the simulation.

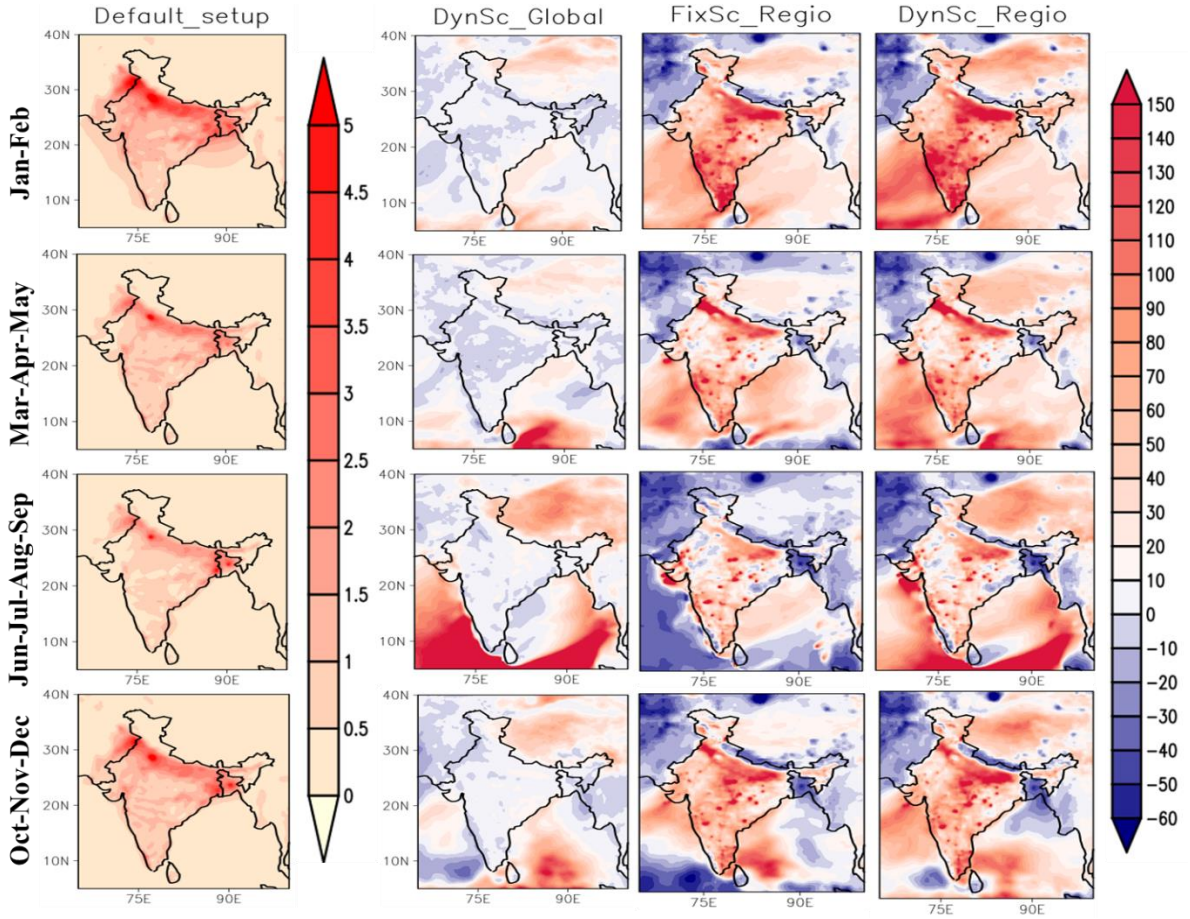

Figure S2. Spatial patterns of mean seasonal surface BC concentration (μg m^{-3}) over India (1st column) using the default set-up and percentage differences in the (2nd and 3rd columns) modified and (4th column customized configurations relative to the default set-up.

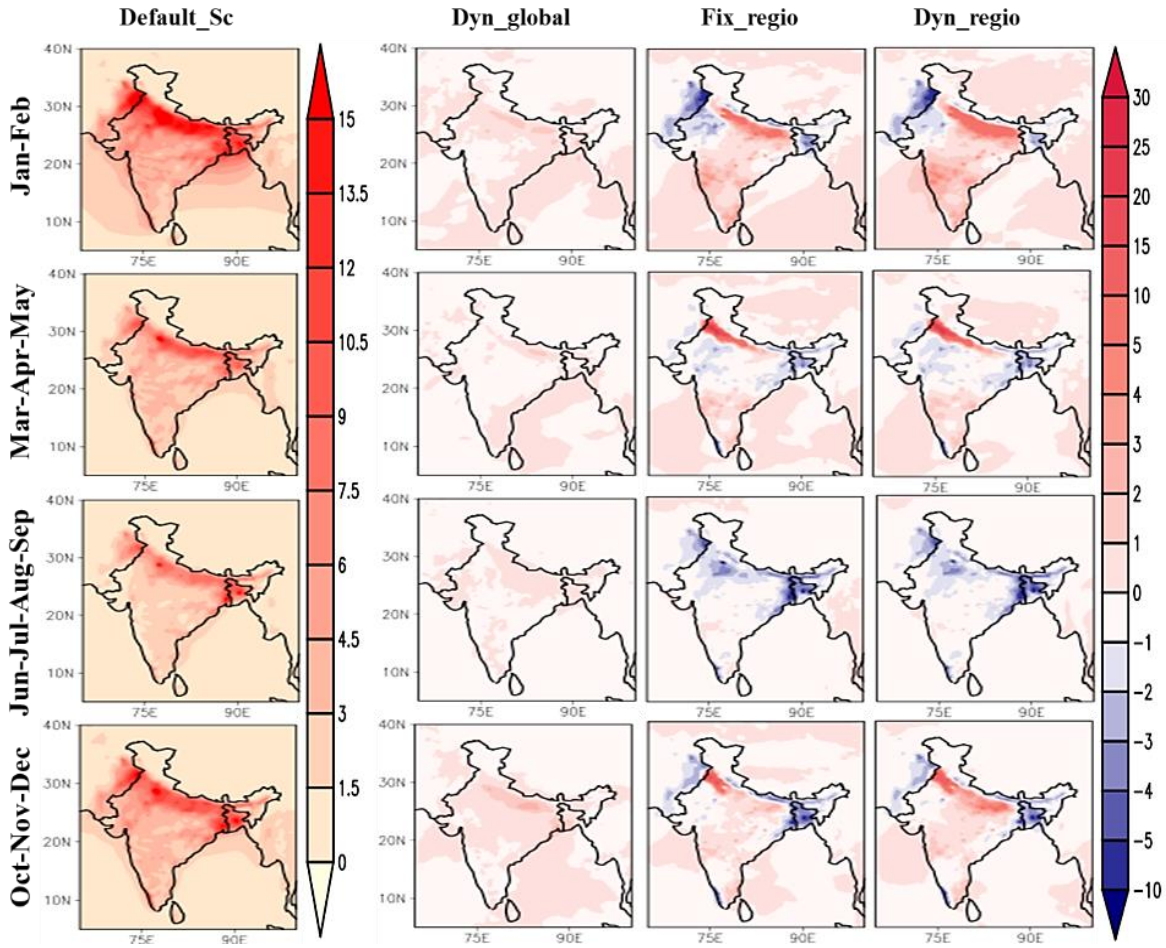

Figure S3. Spatial patterns of mean seasonal surface OC concentration (μg m^{-3}) over India (1st column) using the default set-up and percentage differences in the (2nd and 3rd columns) modified and (4th column customized configurations relative to the default set-up.

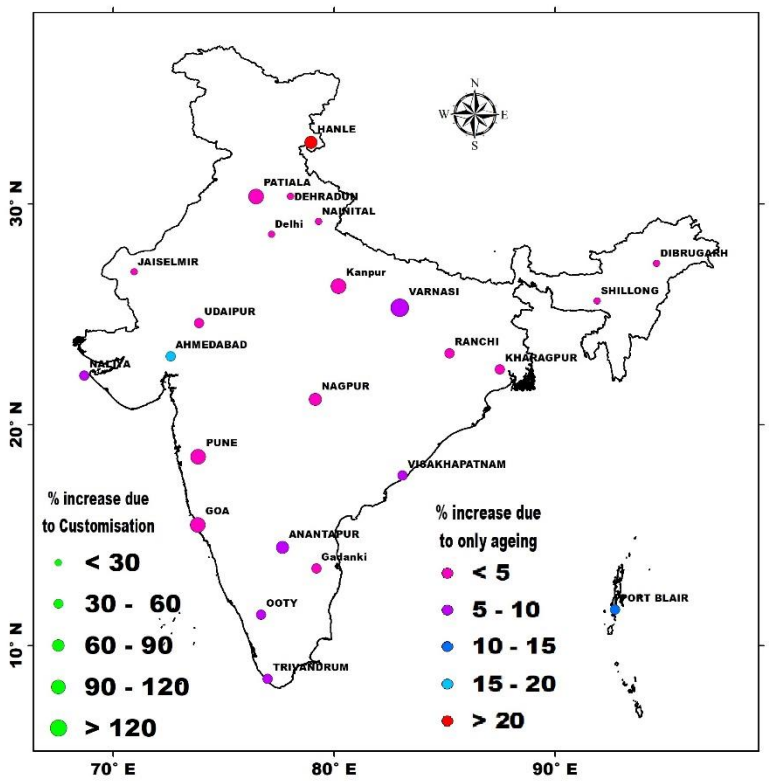

Figure S4. Locations of the 24 cities (Hanle = HNL, Dehradun = DDN, Nainital = NTL, Patiala = PTL, Delhi = DEL, Kanpur = KNP, Varanasi = VNS, Kharagpur = KGP, Ranchi = RNC, Dibrugarh = DBR, Shillong = SHN, Jaisalmer = JSL, Udaipur = UDP, Ahmedabad = AHM, Naliya = NAL, Nagpur = NGP, Pune = PUN, GOA = GOA, Vishakhapatnam = VSK, Gadanki = GAD, Anantpur = ATP, Ooty = OTY, Trivandrum = TVM, Port Blair = PBR) where BC concentrations were measured during the study period and used to evaluate the customized model performance. The colour of the circles indicates the percentage increase in BC concentrations due to the implementation of the dynamic scheme and the size of the circles indicate the percentage increase in BC concentrations due to the combined impact of ageing scheme and regional inventory in the customized model.

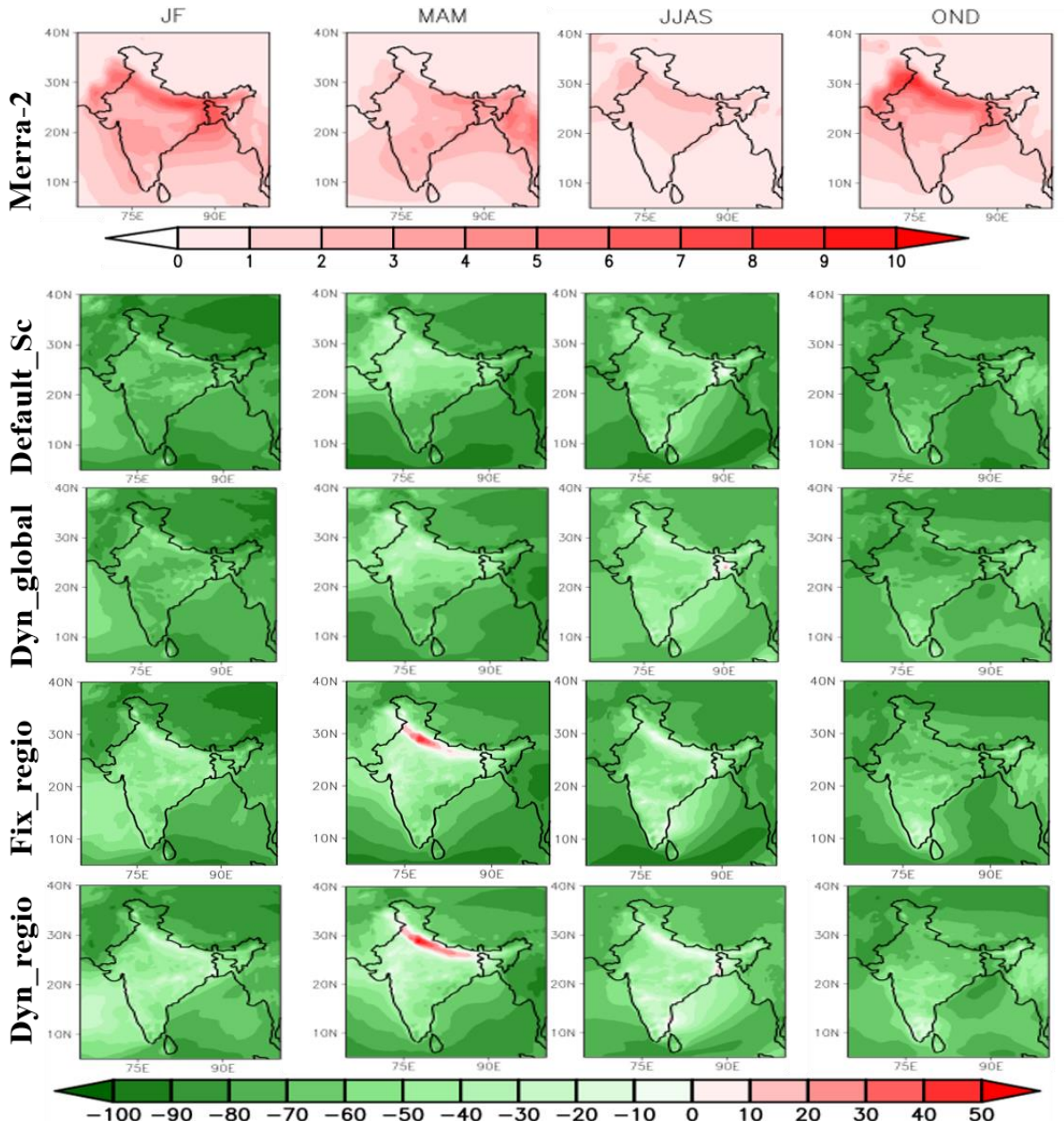

Figure S5. Percentage difference of BC columnar burden simulated by the model w.r.t MERRA-2 BC burden (mg m^{-2}).

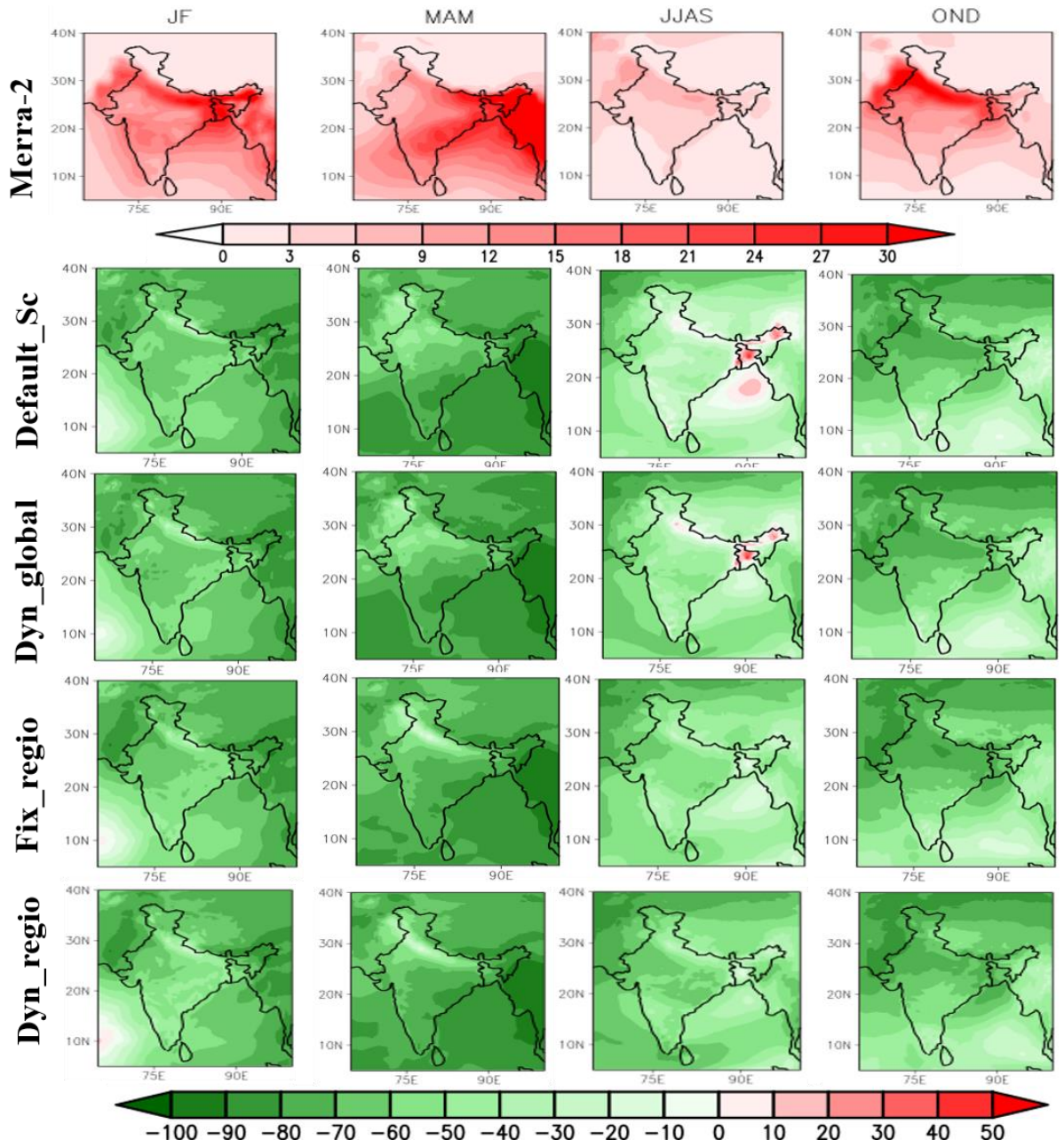

Figure S6. Percentage difference of OC columnar burden simulated by the model w.r.t MERRA-2 OC burden (mg m^{-2}).

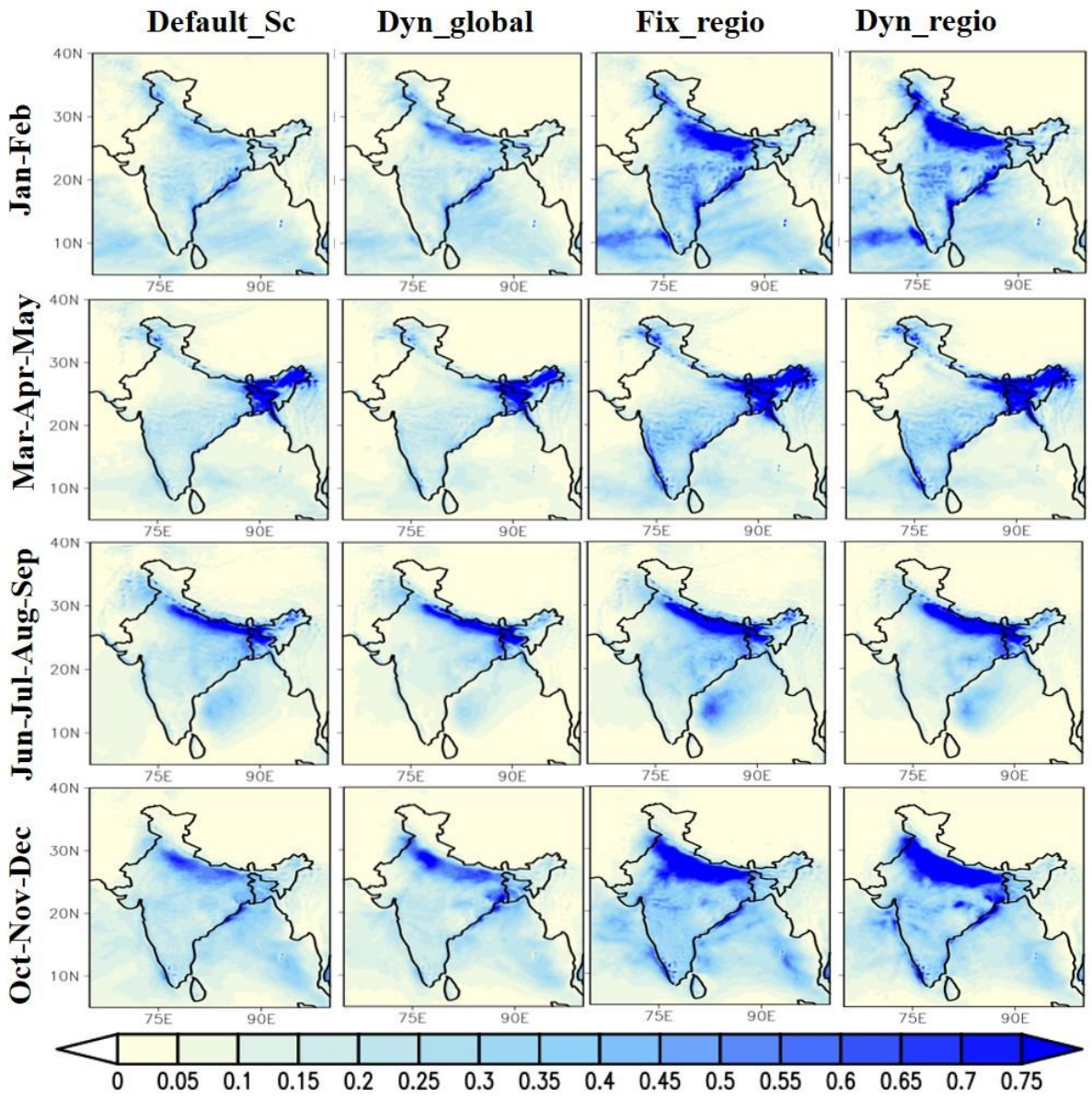

Figure S7. Seasonal distribution of BC_HL wet removal (mg m^{-2} s^{-1}) for four distinct experiments in four seasons.

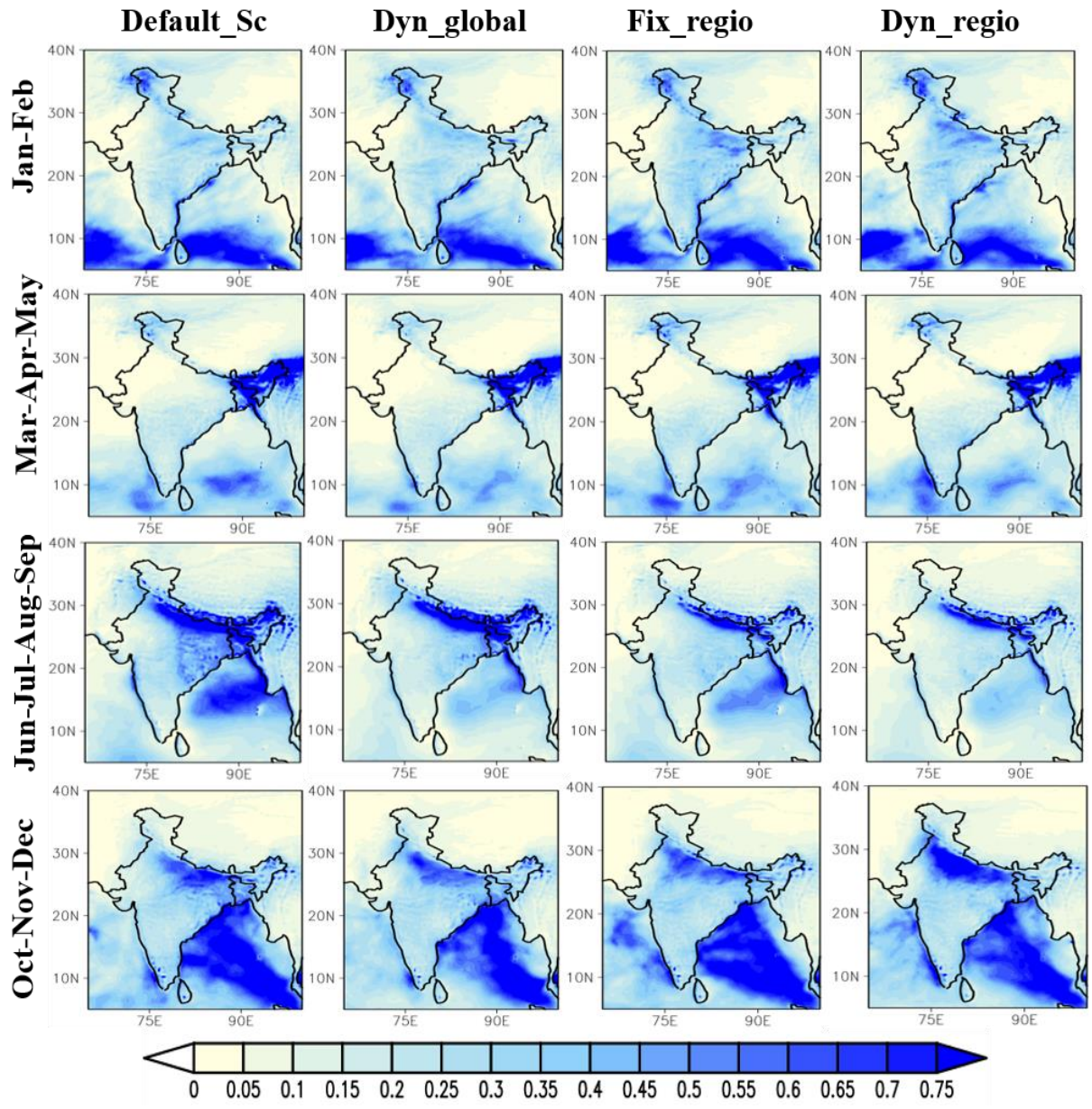

Figure S8. Seasonal distribution of OC_HL wet removal (mg m^{-2} s^{-1}) for four distinct experiments in four seasons.

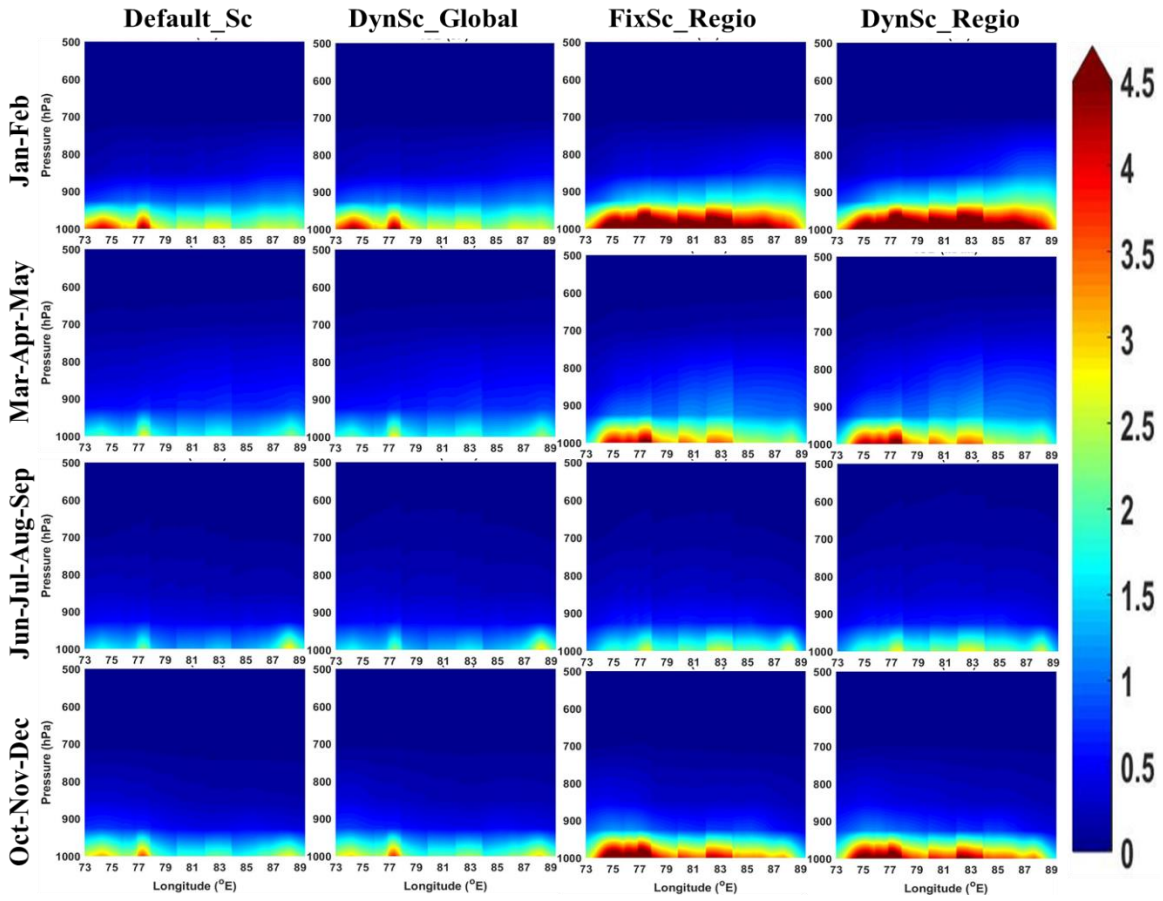

Figure S9. Seasonal variation of vertically distributed mass concentration (μg m^{-3}) of BC over the highly polluted Indo-Gangetic Plain

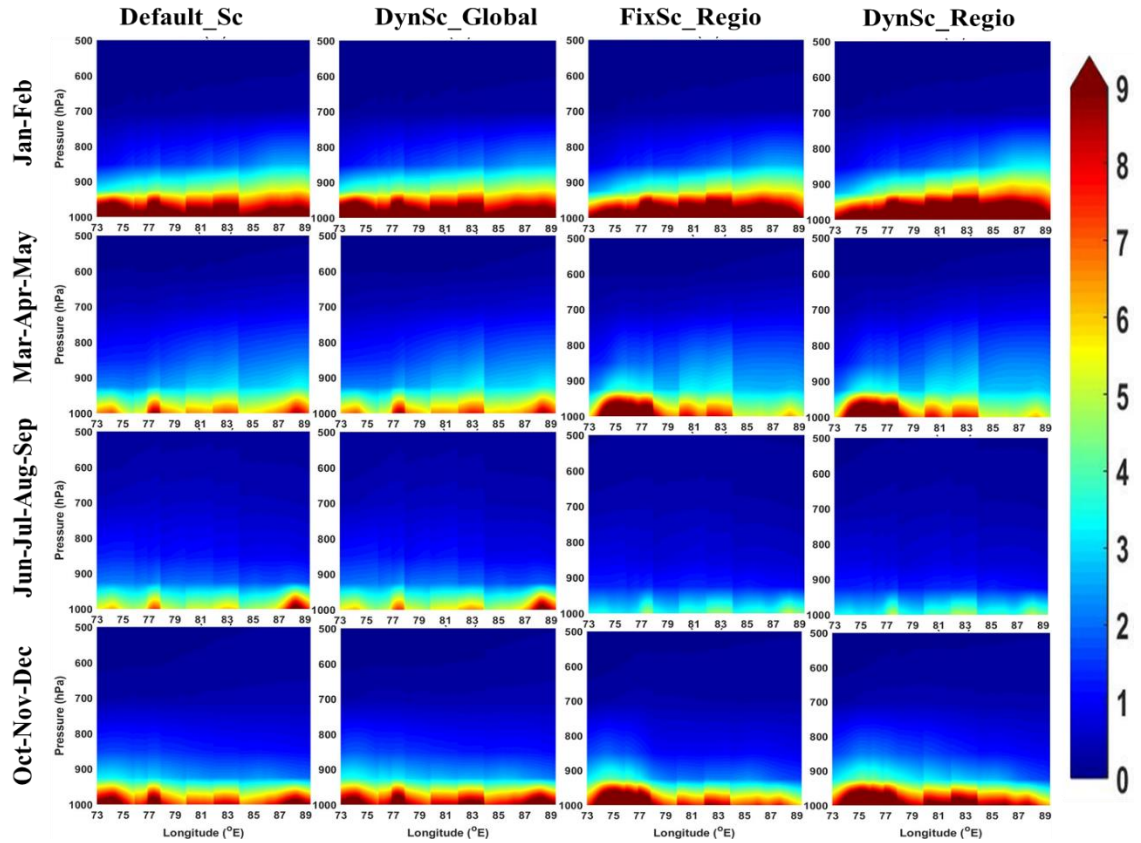

Figure S10. Seasonal variation of vertically distributed mass concentration (μg m^{-3}) of OC over the highly polluted Indo-Gangetic Plain

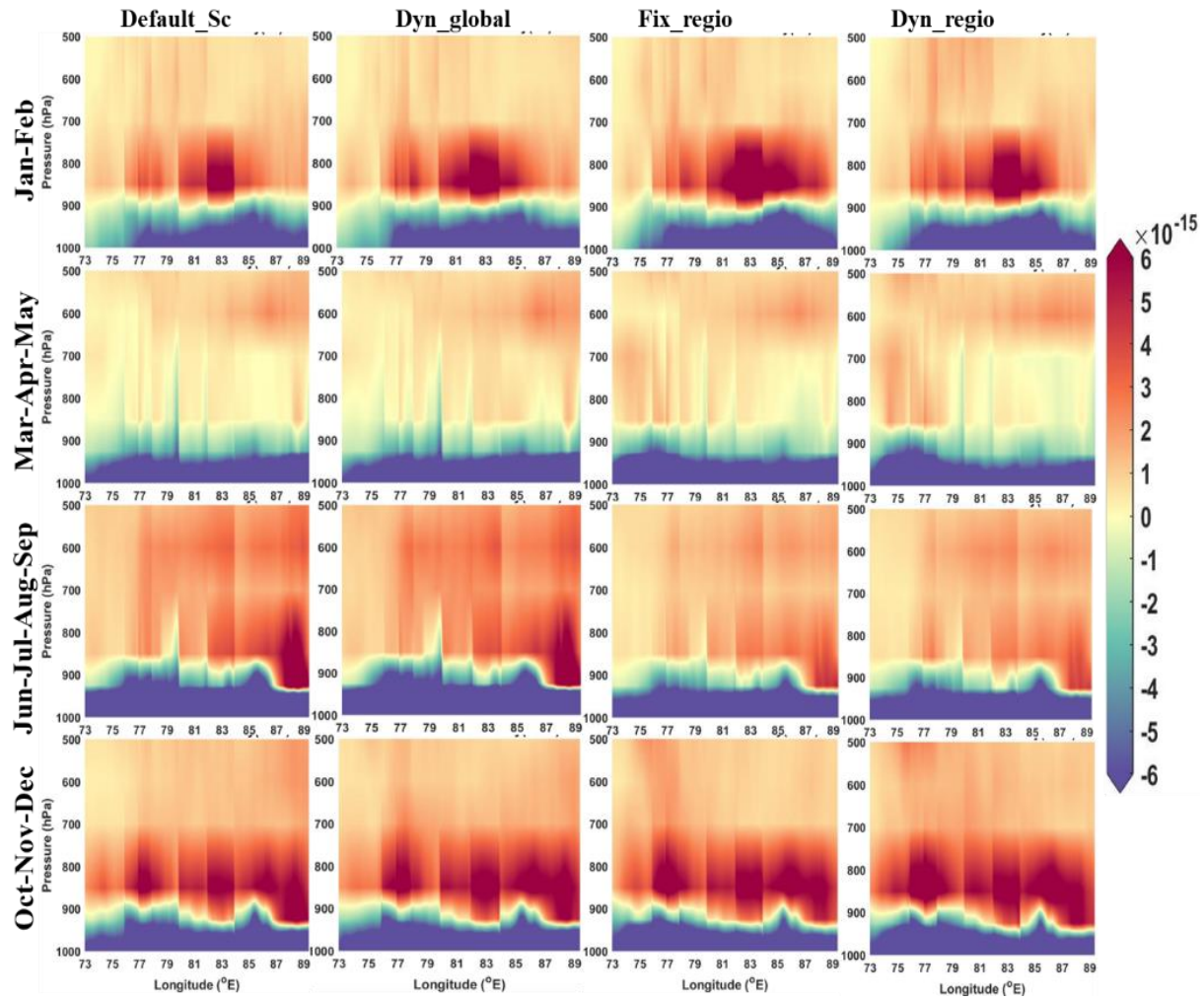

Figure S11. Seasonal distribution of convective tendency (kg kg^{-1} sec^{-1}) of OC over IGP for four distinct experiments.

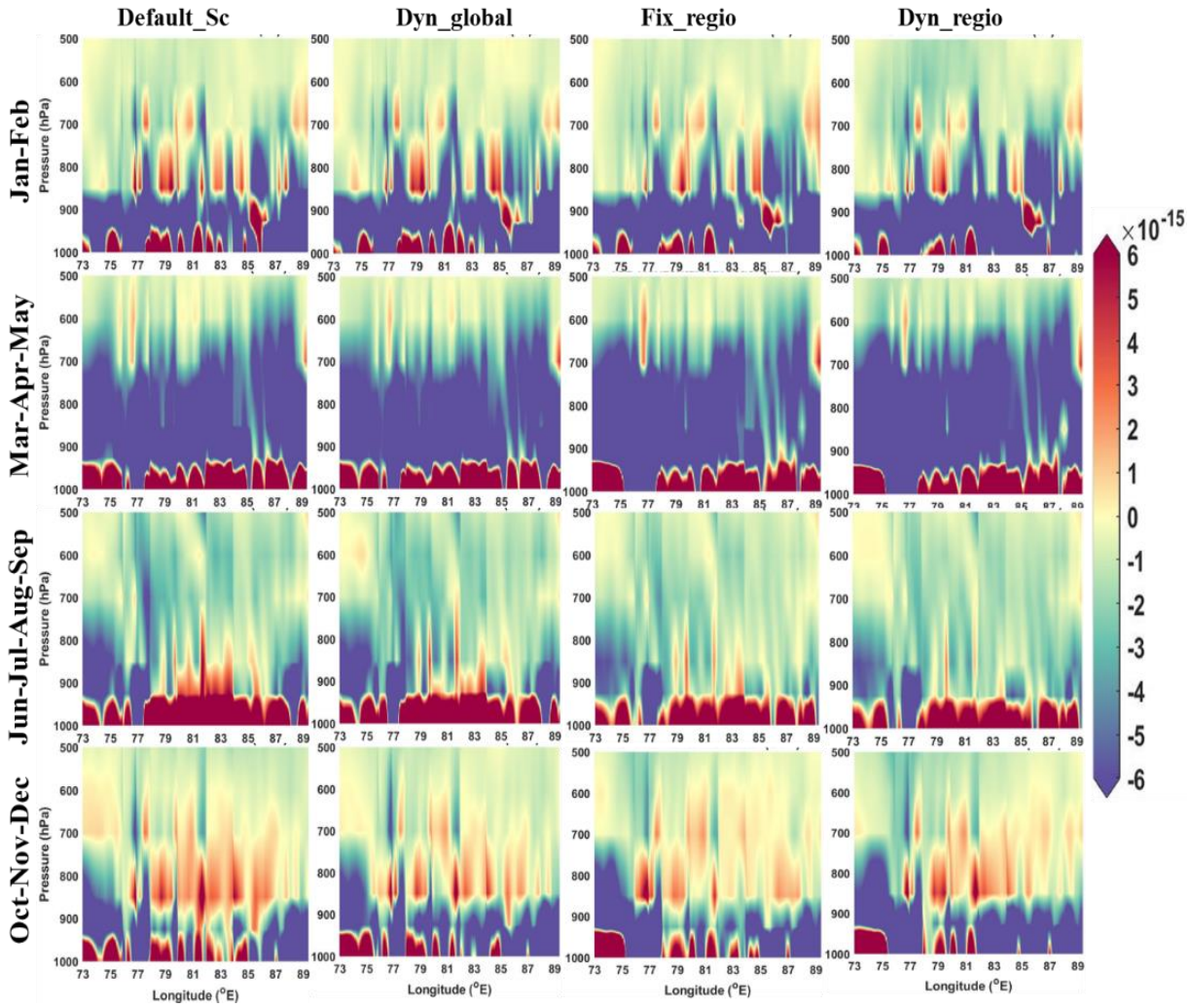

Figure: 12. Seasonal distribution of lateral advection (kg kg^{-1} sec^{-1}) of OC over IGP for four distinct experiments.

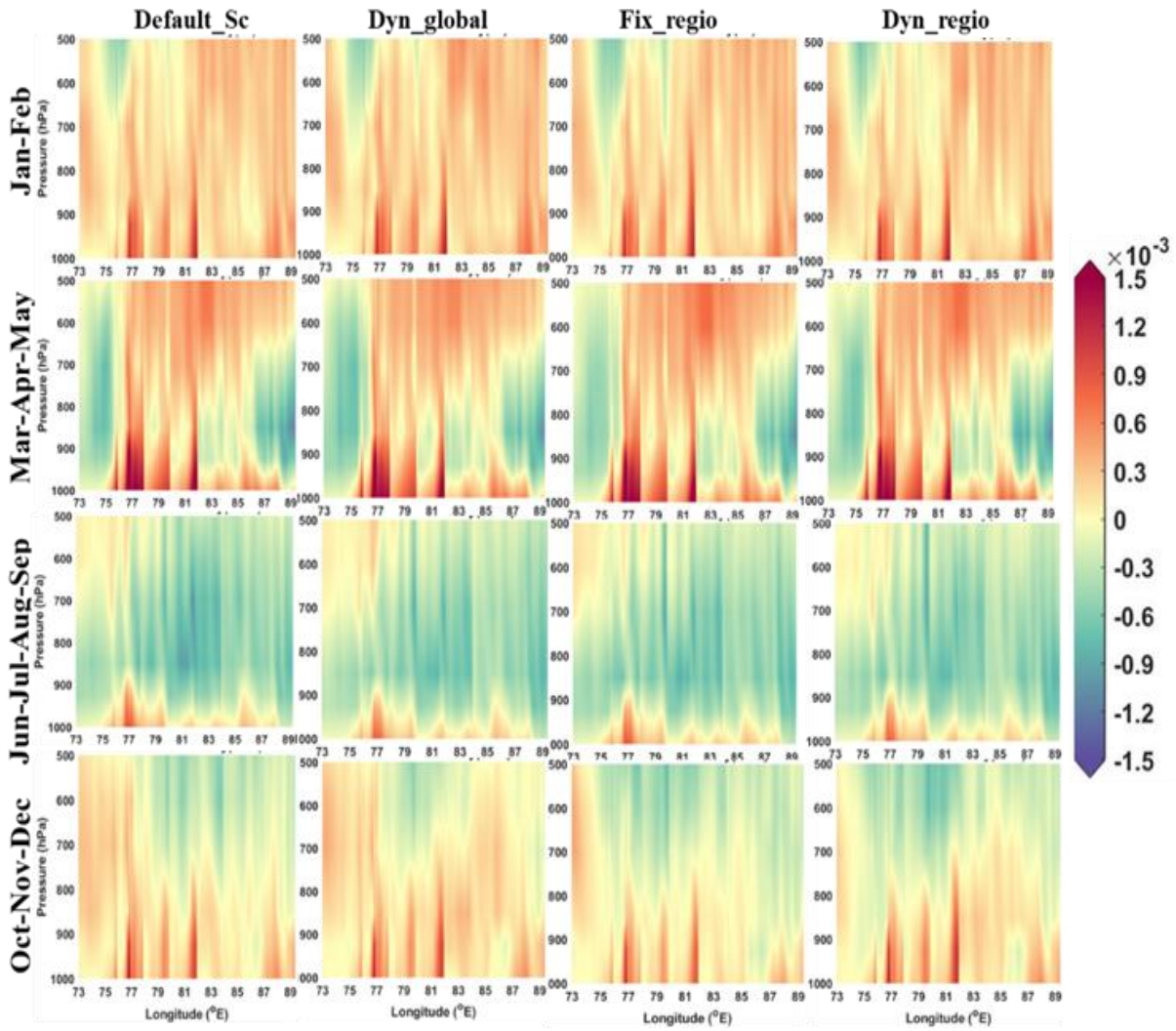

Figure S13 Seasonal distribution of vertical wind, omega (in m sec^{-1}) over IGP for four distinct experiments.

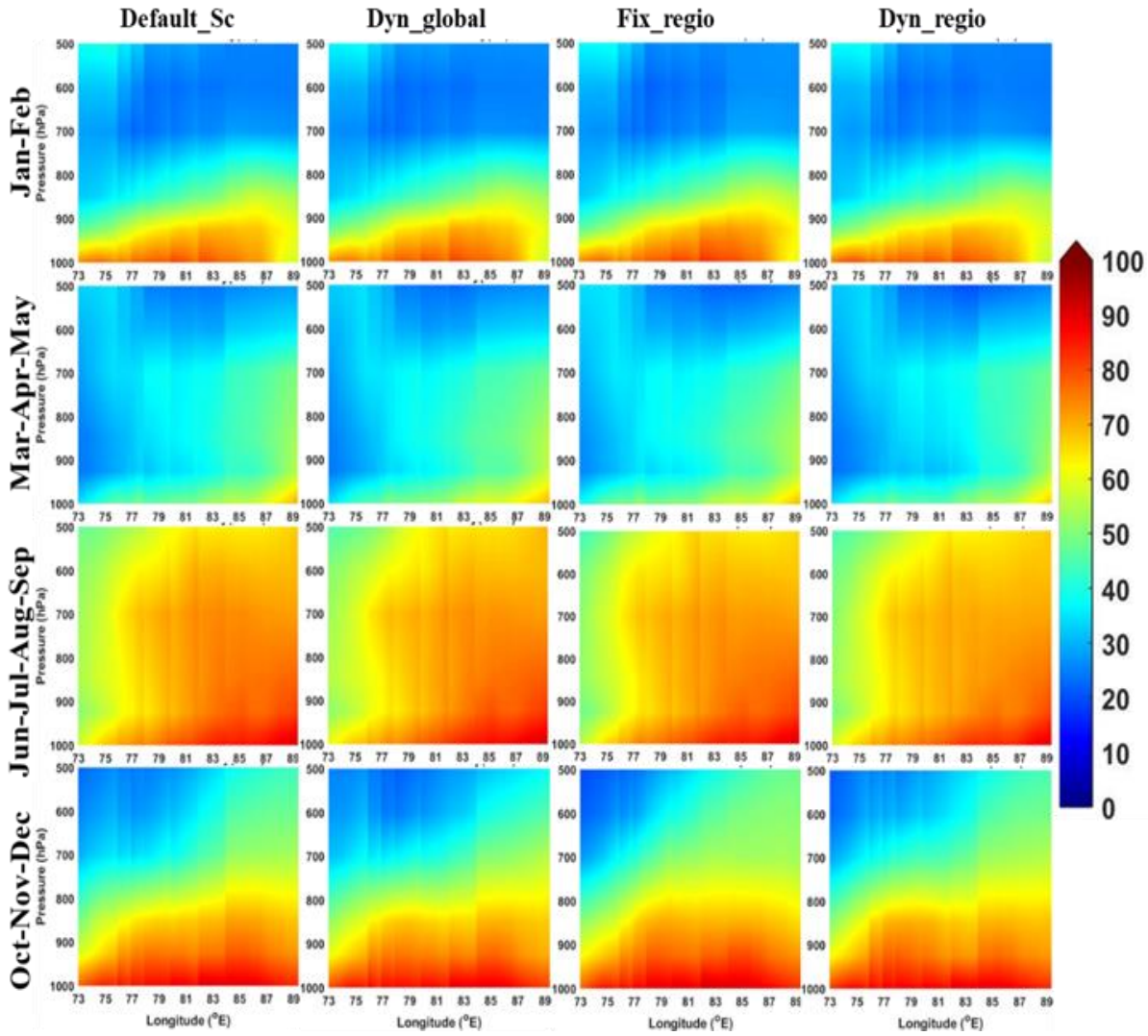

Figure S14 Seasonal distribution of relative humidity (%RH) over Indo-Gangetic Basin (IGP) for the four distinct experiments.

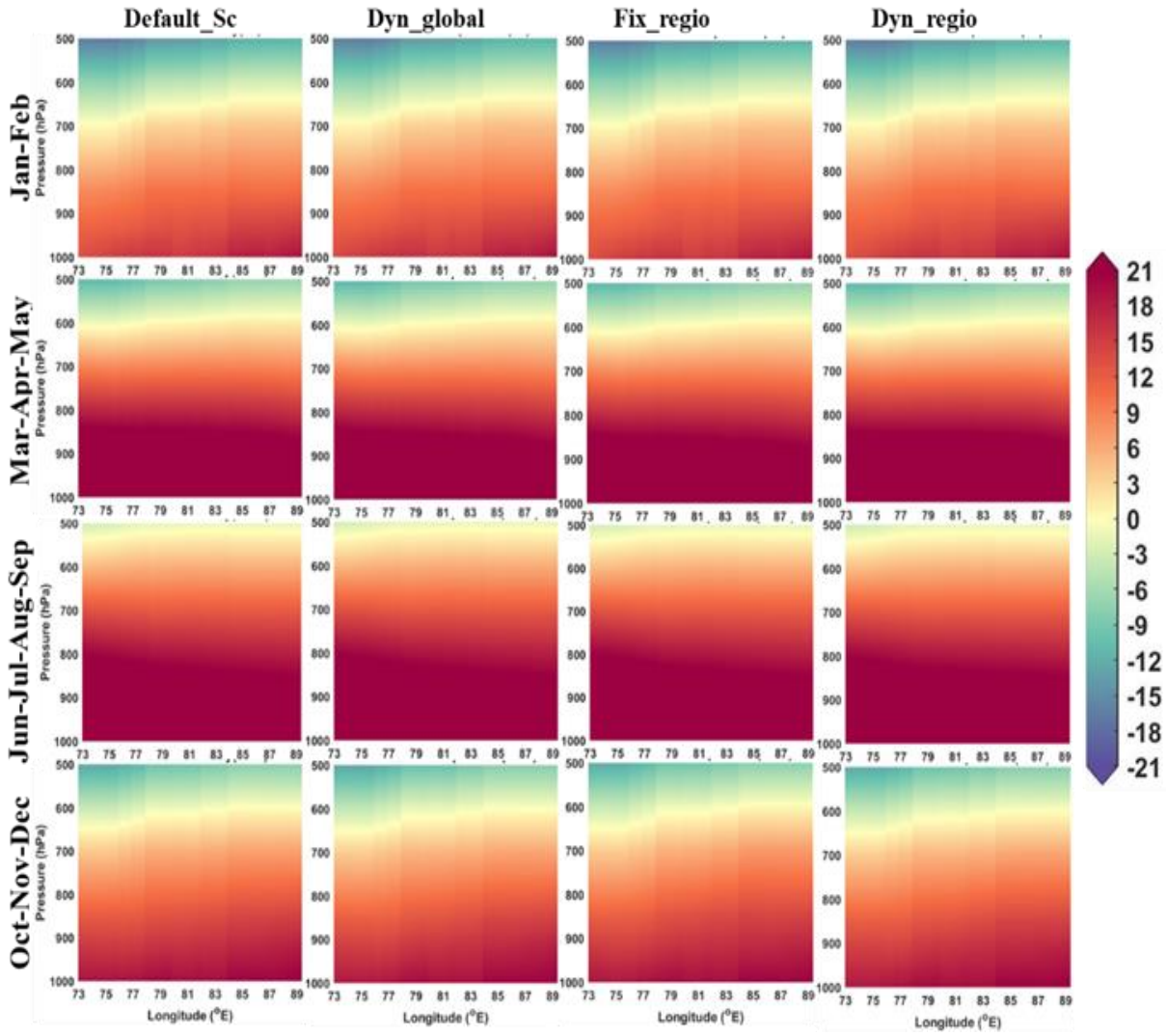

Figure S15. Seasonal distribution of temperature (in °C) over IGP for four distinct experiments.

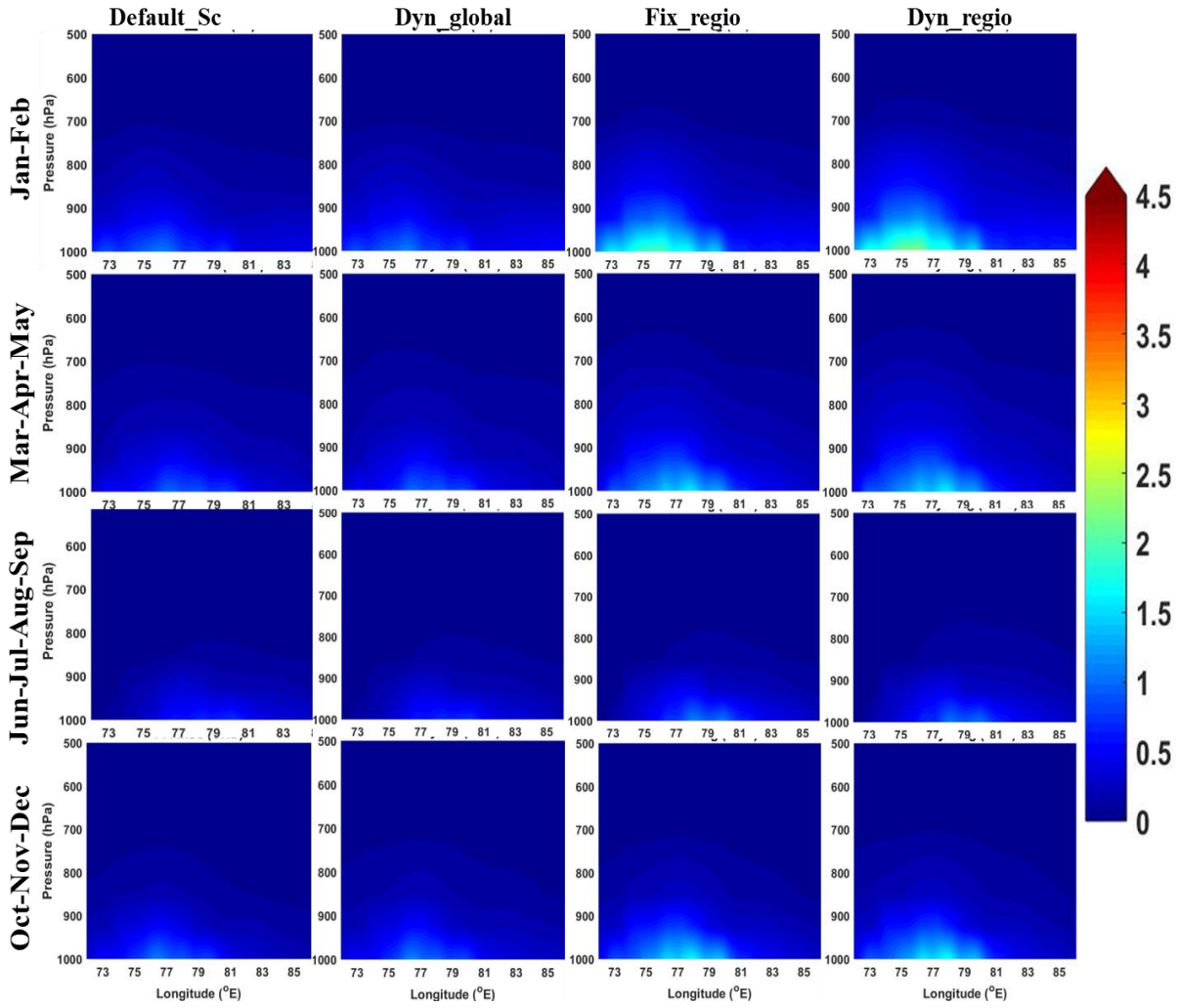

Figure S16. Seasonal variation of vertically distributed mass concentration (μg m^{-3}) of BC over PI.

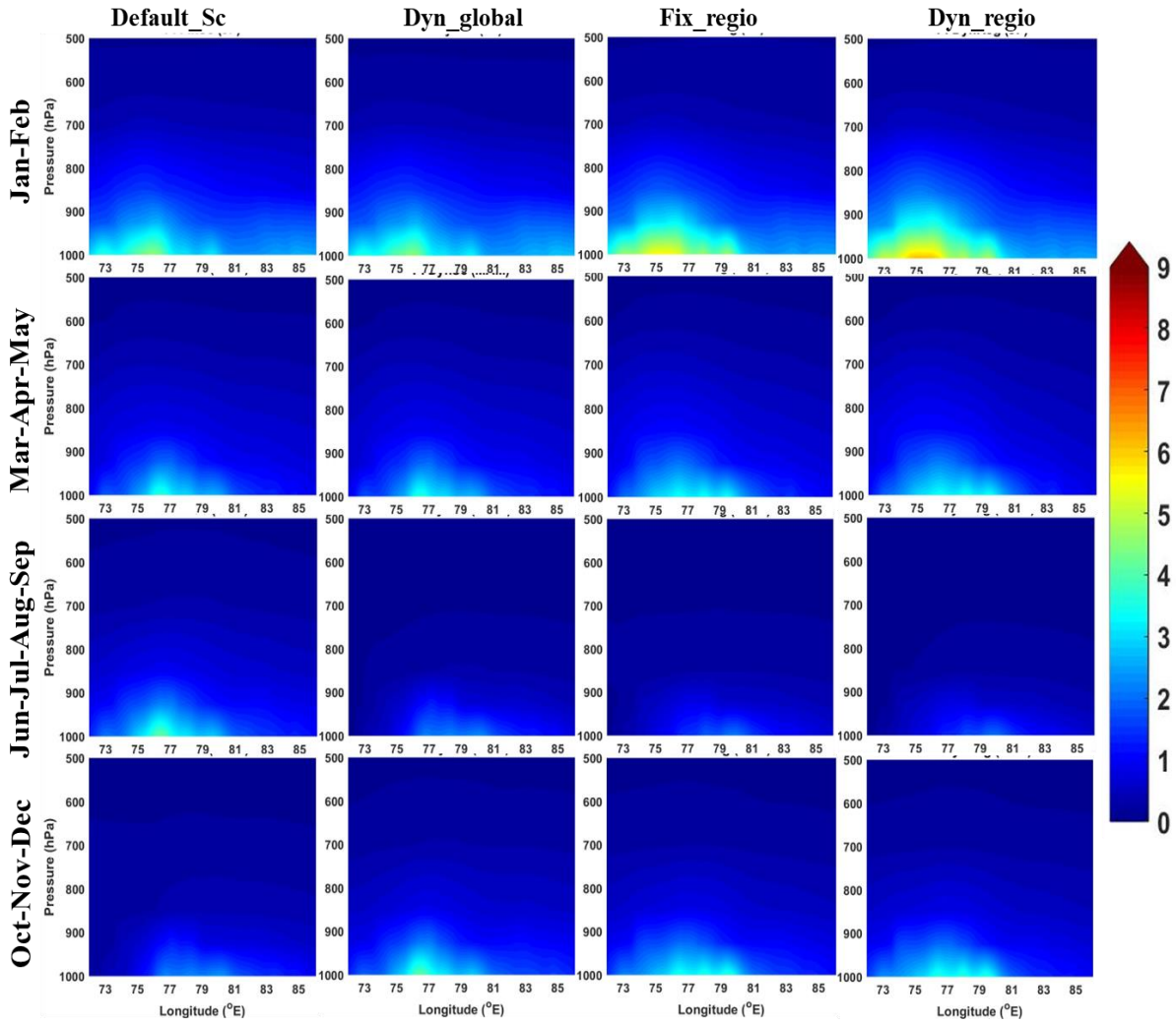

Figure S17. Seasonal variation of vertically distributed mass concentration (μg m^{-3}) of OC over PI.

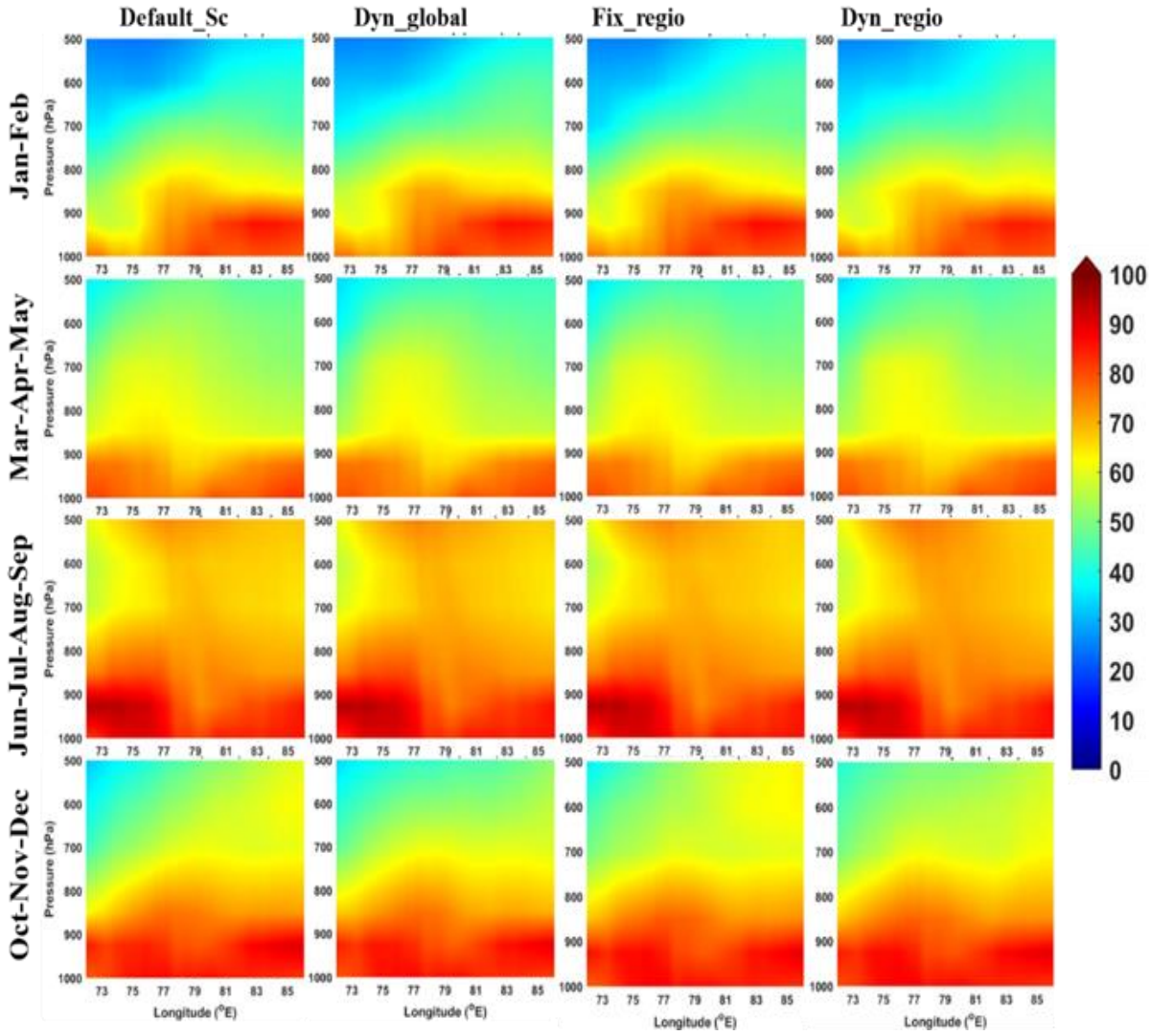

Figure S18. Seasonal distribution of relative humidity (%RH) over Peninsular India (PI) for the four distinct experiments.

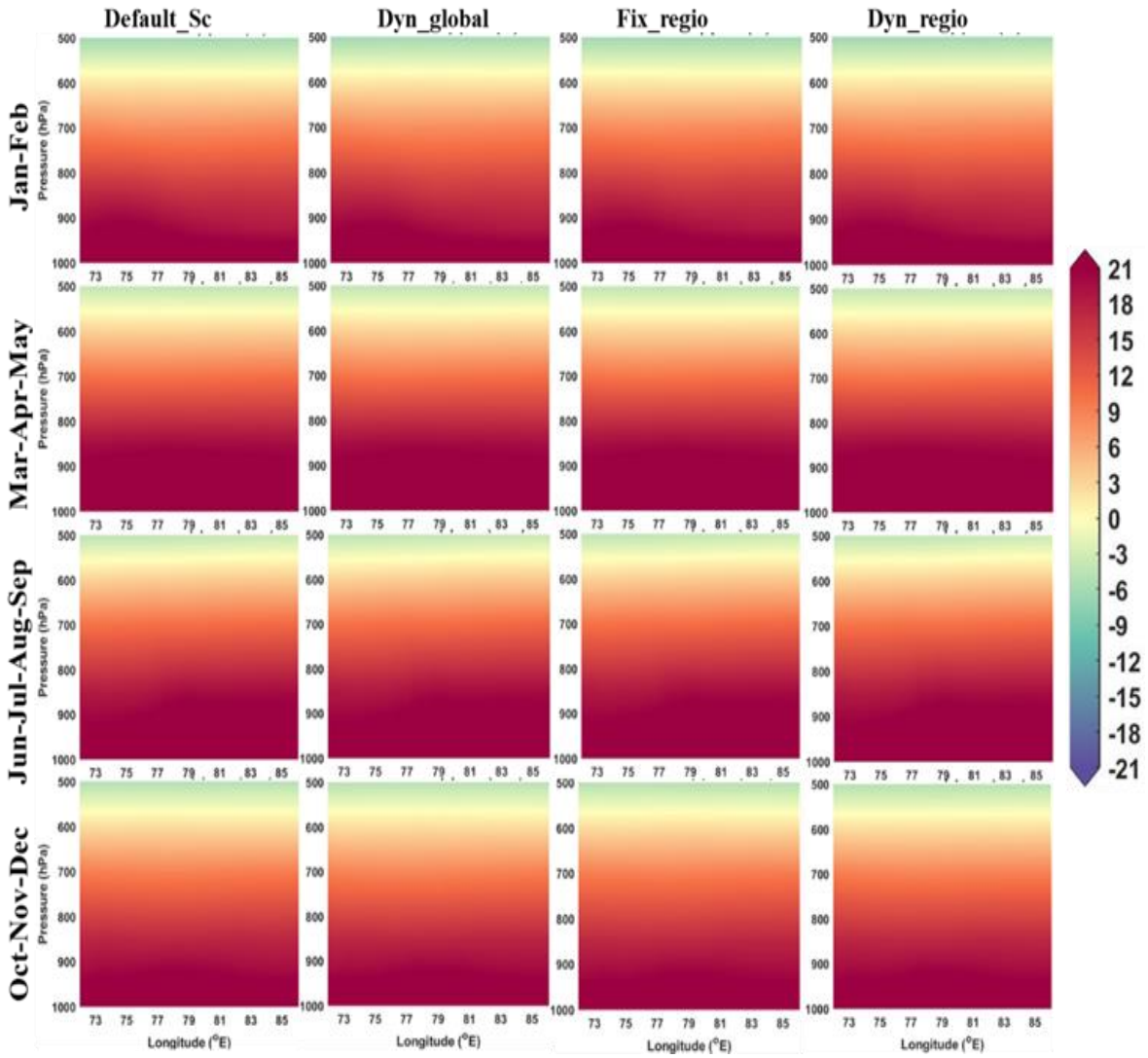

Figure S19. Seasonal distribution of 2m air temperature (in °C) over PI for four distinct experiments.

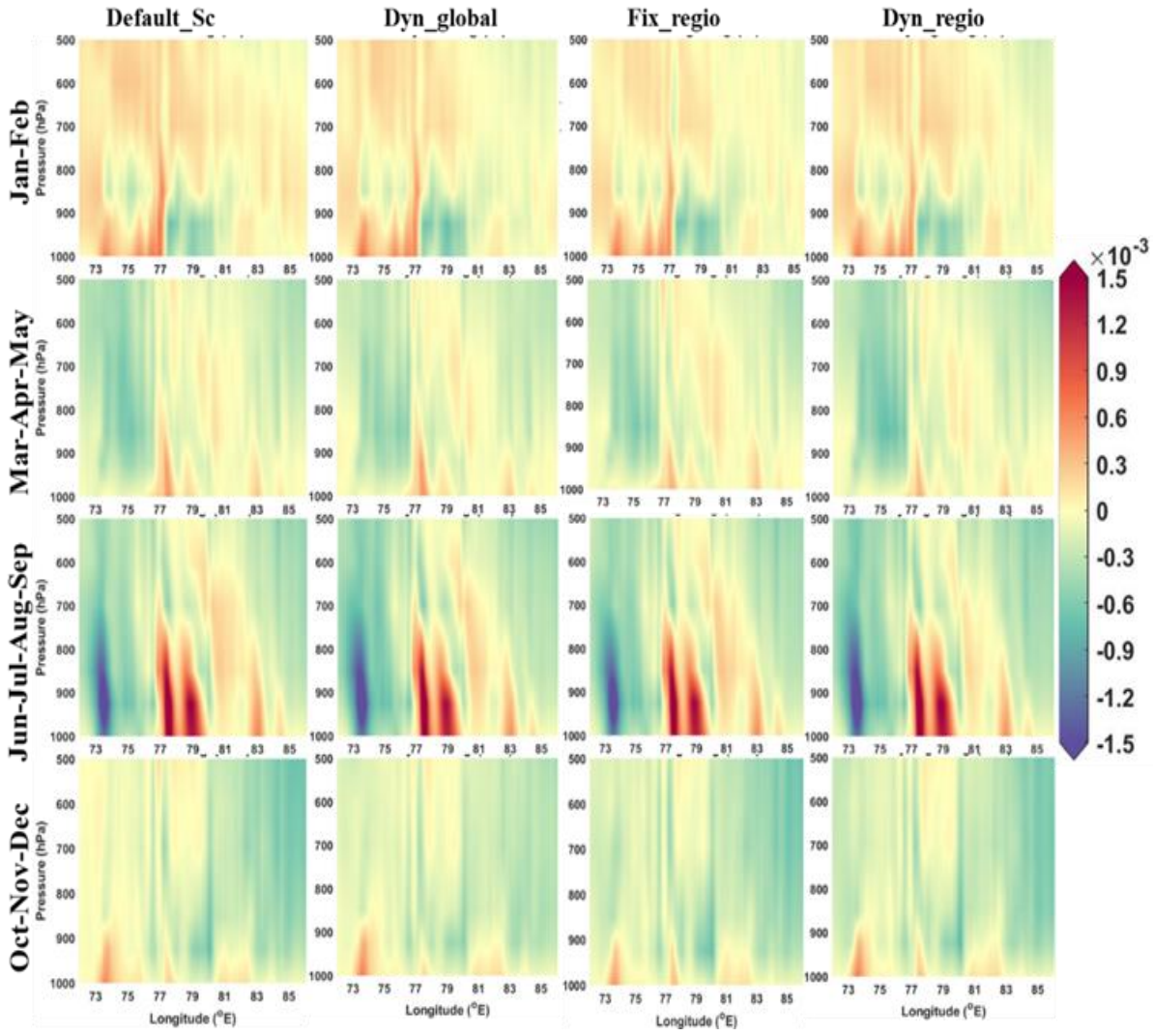

Figure S20. Seasonal distribution of vertical wind, omega (in m sec^{-1}) over PI for four distinct experiments.

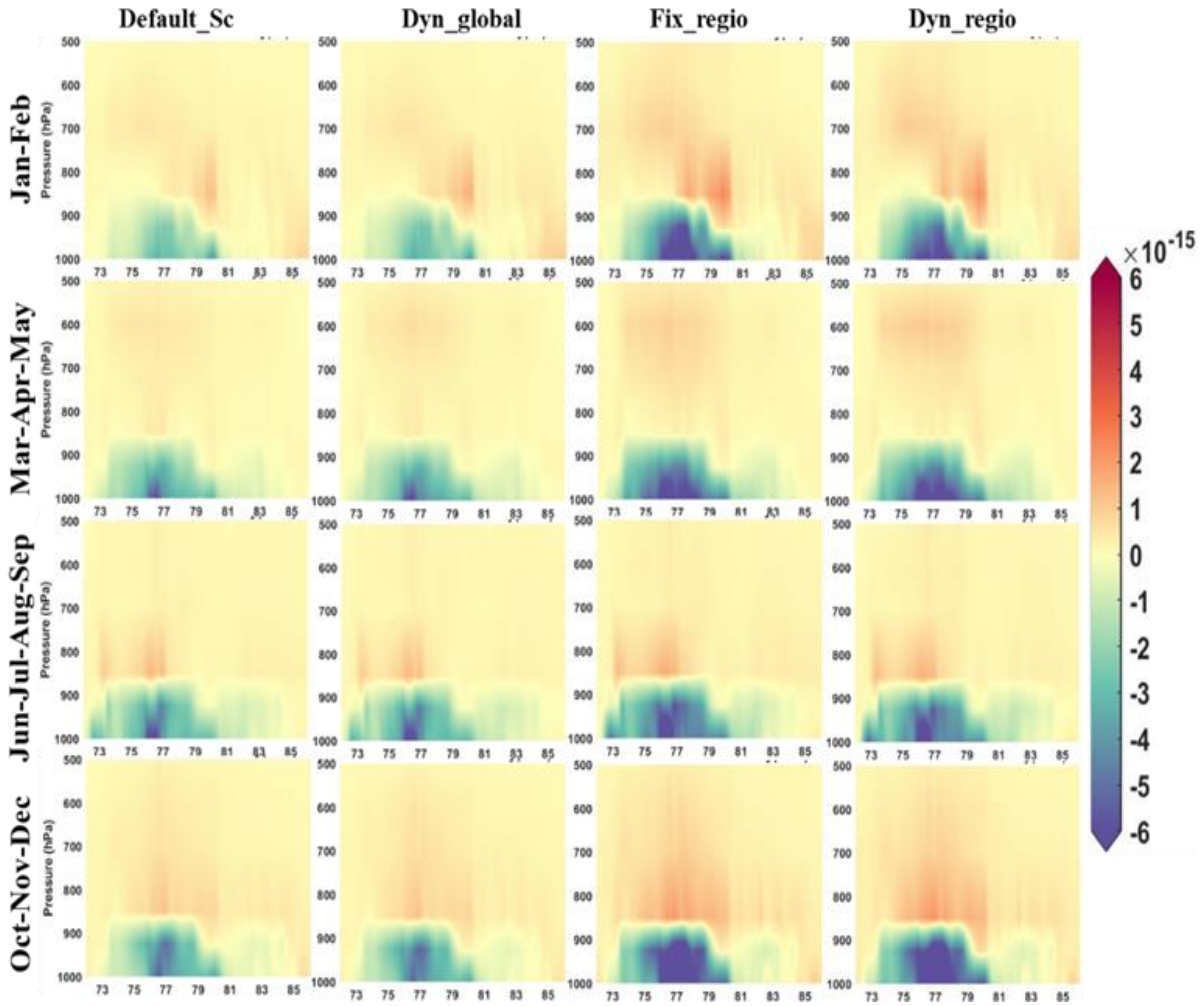

Figure S21 Seasonal distribution of convective tendency (kg kg^{-1} sec^{-1}) of BC over PI for four distinct experiments.

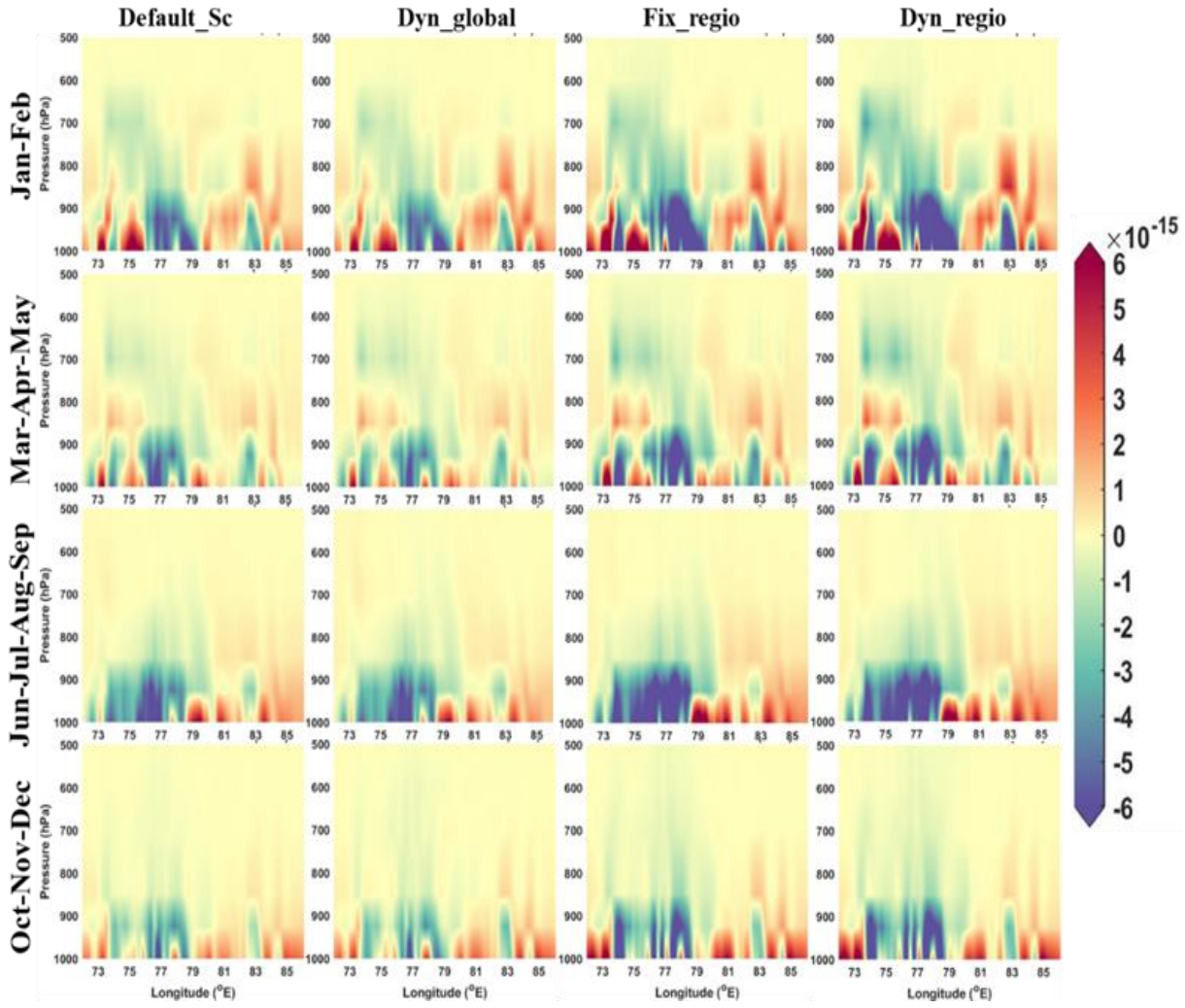

Figure S22 Seasonal distribution of lateral advection (kg kg^{-1} sec^{-1}) of BC over PI for four distinct experiments.

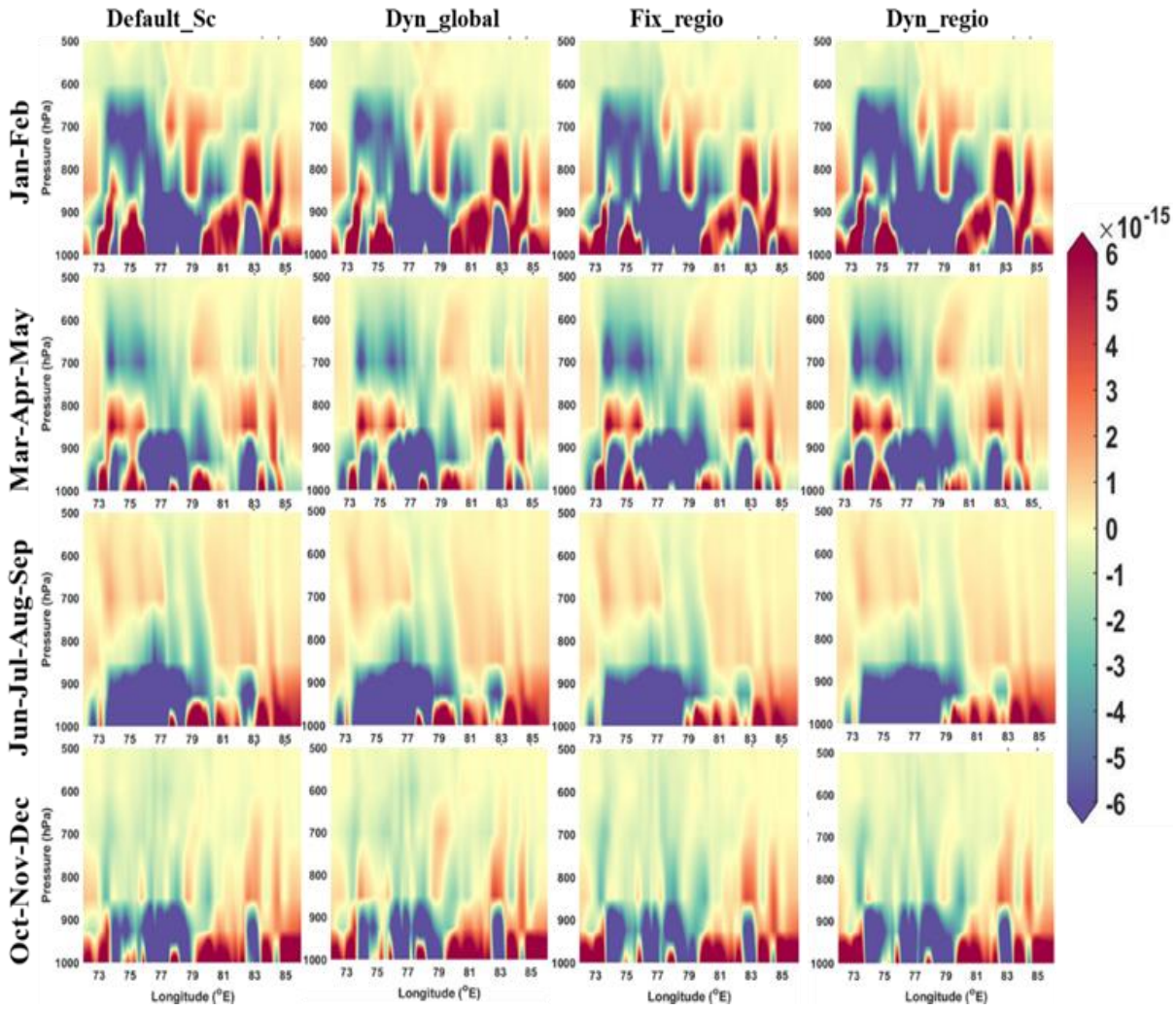

Figure S23 Seasonal distribution of lateral advection (kg kg^{-1} sec^{-1}) of OC over PI for four distinct experiments.

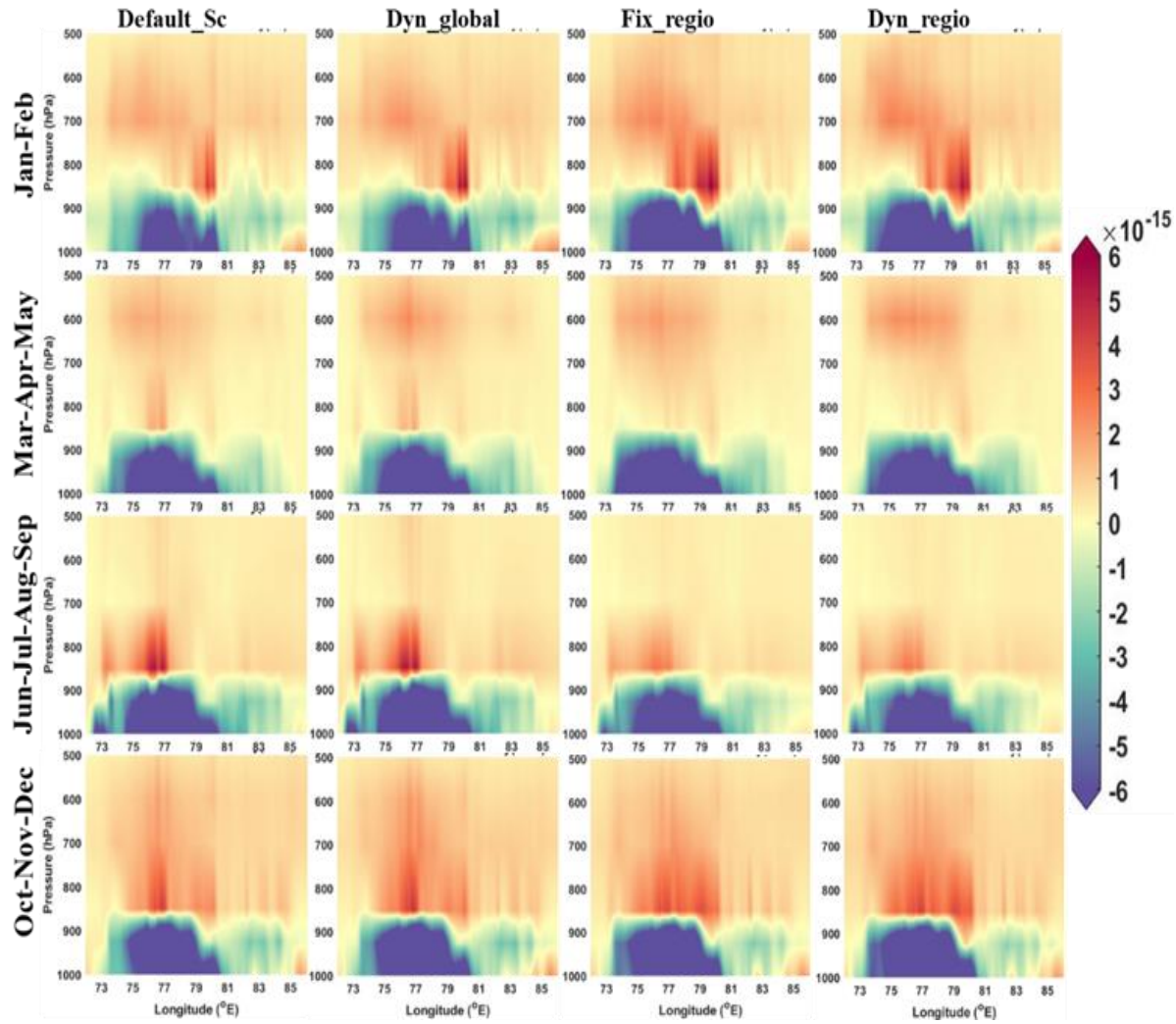

Figure S24 Seasonal distribution of convective tendency (kg kg^{-1} sec^{-1}) of OC over PI for four distinct experiments.

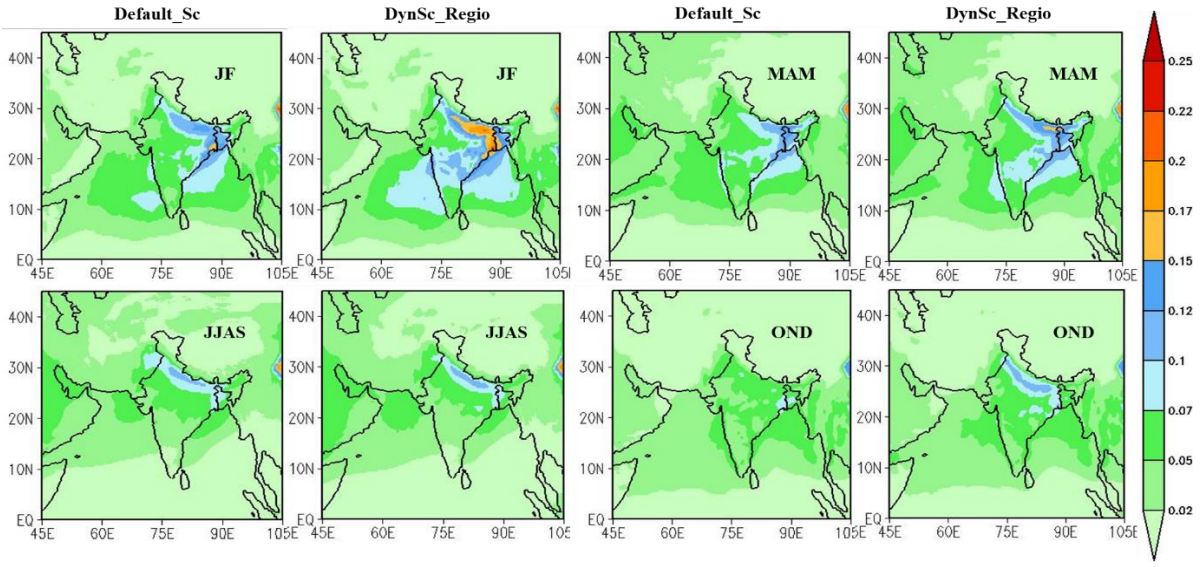

Figure S25: Seasonal variation of anthropogenic aod simulated by default and augmented model set-up.

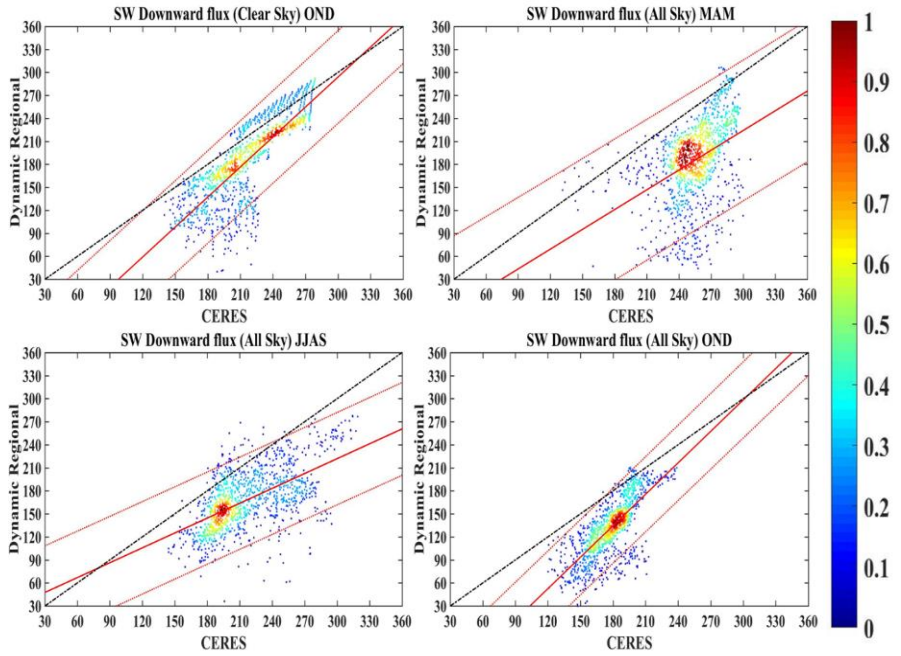

Figure S26: Evaluation between model derived surface downward shortwave flux and CERES surface shortwave flux (W m^{-2}) for all-sky conditions for the year 2010. Black line represents 1:1 line and solid red line is the curve fitting line along with red dotted predicted bounds.

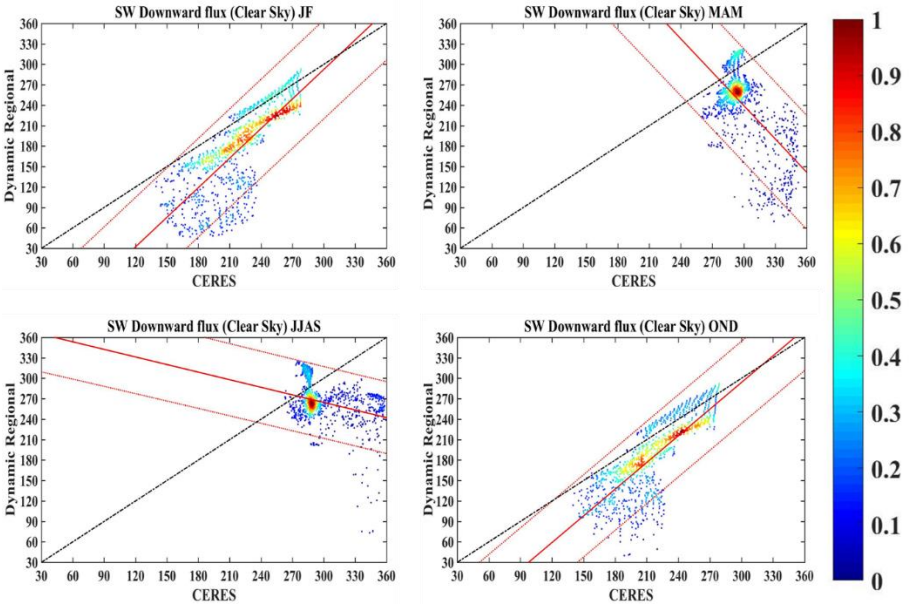

Figure S27: Evaluation between model derived surface downward shortwave flux and CERES surface shortwave flux (W m^{-2}) for all-sky conditions for the year 2010. Black line represents 1:1 line and solid red line is the curve fitting line along with red dotted predicted bounds.